Dehydrogenation of goethite in Earth's deep lower mantle

Qingyang Hu[a,b,c,1], Duck Young Kim[a,1], Jin Liu[b,1], Yue Meng[d], Liuxiang Yang[a,c], Dongzhou Zhang[e], Wendy L. Mao[b], and Ho-kwang Mao[a,c,2]

[a]Center for High Pressure Science and Technology Advanced Research, Shanghai 201203, People's Republic of China; [b]Department of Geological Sciences, Stanford University, Stanford, CA 94305; [c]Geophysical Laboratory, Carnegie Institution, Washington, DC 20015; [d]High Pressure Collaborative Access Team, Geophysical Laboratory, Carnegie Institution, Argonne, IL 60439; and [e]Hawaii Institute of Geophysics and Planetology, School of Ocean and Earth Science and Technology, University of Hawaii at Manoa, Honolulu, HI 96822

The cycling of hydrogen influences the structure, composition, and stratification of Earth's interior. Our recent discovery of pyrite-structured iron peroxide (designated as the P phase) and the formation of the P phase from dehydrogenation of goethite FeO_2H implies the separation of the oxygen and hydrogen cycles in the deep lower mantle beneath 1,800 km. Here we further characterize the residual hydrogen, x, in the P-phase FeO_2Hx. Using a combination of theoretical simulations and high-pressure–temperature experiments, we calibrated the x dependence of molar volume of the P phase. Within the current range of experimental conditions, we observed a compositional range of P phase of $0.39 < x < 0.81$, corresponding to 19–61% dehydrogenation. Increasing temperature and heating time will help release hydrogen and lower x, suggesting that dehydrogenation could be approaching completion at the high-temperature conditions of the lower mantle over extended geological time. Our observations indicate a fundamental change in the mode of hydrogen release from dehydration in the upper mantle to dehydrogenation in the deep lower mantle, thus differentiating the deep hydrogen and hydrous cycles.

dehydrogenation | high pressure | P phase | FeO_2 | FeO_2H

In Earth's crust and down through the mantle transition zone, hydrogen exists primarily in its oxidized form. Hydrogen in hydrous minerals subducts with down-going slabs and reemerges from the upper mantle as water in island arc volcanic volatiles, maintaining its oxidized form. The deep hydrogen cycle is thus often tied to the water cycle (1–3). A growing number of studies have reported that hydrogen can be transported deeper into the lower mantle by close-packed hydrous minerals, including: δ-AlO_2H (4, 5), phase H ($MgSiO_4H_2$) (6–8), aluminum-enriched silicates (9), and ε-FeO_2H (10), extending the hydrogen–hydrous cycle to the entire mantle. However, how hydrogen in the deep lower mantle returns to Earth's surface is less explored. Would the hydrogen return as water by dehydration of the hydrous minerals or as hydrogen by dehydrogenation (11)? The return of hydrogen is a critical control on the redox equilibria in the mantle.

Our previous work shows that a common hydrous mineral, goethite FeO_2H, dehydrogenates to form the pyrite-structured P phase at deep lower mantle conditions (12). The P phase resulting from dehydrogenation has variable, larger unit cells than pure FeO_2, suggesting that it may retain $x < 1$ amount of hydrogen in the form of FeO_2Hx. In light of this, we are motivated to quantify the dehydrogenation reaction of FeO_2H. First-principles calculations were used to further constrain and quantify the hydrogen content in the FeO_2Hx P phase.

Results

High P-T experiments on FeO_2H were conducted in a diamond anvil cell (DAC) integrated with laser heating. The starting materials were either precompressed goethite (α-FeO_2H) powders in Ar or Ne pressure media or hematite (Fe_2O_3) in water pressure medium that is chemically equivalent to goethite as $Fe_2O_3 + H_2O = 2FeO_2H$ (13, 14). Samples were gradually compressed to the target pressure

range of 71–133 GPa, before being heated by a double-sided neodymium-doped yttrium aluminium garnet (Nd: YAG) laser up to 10 min (15). Using a synchrotron X-ray diffraction (XRD) technique, the cubic P phase was identified to form above 72 GPa and preserved in the temperature-quenched sample (Fig. 1 A–C). The P phase was stable at least up to 133 GPa and 2,000 K (Fig. 1D). The formation of the P phase was well reproduced in all experiments with a variety of samples and media (Table 1) over a wide pressure range.

In our experiments, P phase decomposed from FeO_2H had the identical space group to FeO_2, but had a larger and variable unit cell volume, depending on the amount of hydrogen loss in the nonstoichiometric P phase. The key issue, therefore, is to determine the range of x in FeO_2Hx. The baseline $x = 0$ can be accurately defined by the pure FeO_2 that was synthesized from the reaction of Fe_2O_3 in a pure oxygen environment free of hydrogen. Results of FeO_2 were consistent with our previous work (12) and the details of synthesis can be found in Materials and Methods.

The other boundary condition, $x = 1$, however, is much harder to pin down. Many signs, such as the observations of the hydrogen vibron in Ne and the presence of metastable iron hydride, indicate that the formation of the P phase always alters the FeO_2H composition by loss of some H. We performed first-principles simulations on FeO_2H to help us to define the upper limit with $x = 1$. In fully hydrogenated FeO_2H, our 0-K calculation showed it stabilized in the same structure as pyrite-type $AlOOH$ (16) and pyrite-FeO_2 (12). Unlike many hydrous phases that form hydroxyl (6, 8), hydrogen atoms in the P phase are equally bonded with two oxygen atoms that significantly soften the O-H stretching and bending mode compared with iron hydroxides (17) (Fig. S1).

The molar volume of P phase as a function of pressure from experiments and simulations was plotted in Fig. 2. The volumes of

Significance

We found at high pressure–temperature (*P-T*) that the goethite FeO_2H transforms to P-phase FeO_2 via a two-step dehydrogenation process. First it releases some hydrogen to form P-phase FeO_2Hx, and then it continuously releases the remaining hydrogen through prolonged heating. This work provides an important example that the dehydration reaction changes to dehydrogenation of FeO_2H at the lower mantle conditions and the cycles of hydrogen and water become separated.
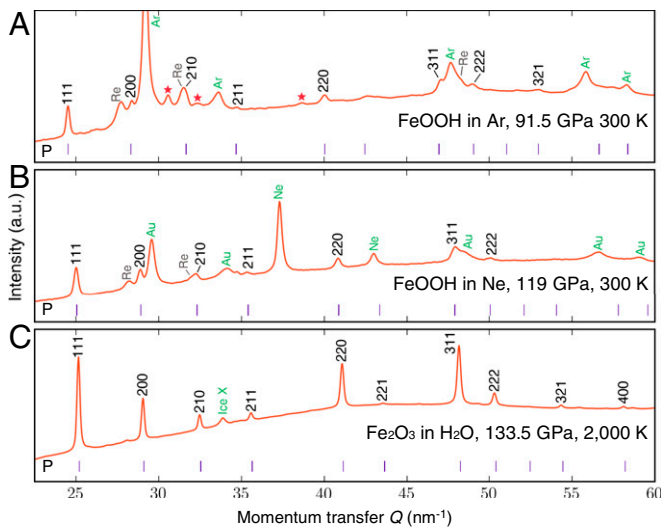
Fig. 1. Selected in situ XRD patterns of the P phase. (A) FeOOH in Ar at 91.5 GPa and quenched to 300 K. (B) FeOOH in Ne at 119 GPa and quenched to 300 K. (C) In situ at 133 GPa and 2,000 K for Fe_2O_3 and water assemblage. Tick marks at the bottom and *hkl* labels are the calculated peak positions for the P phase. The green labels indicate diffraction from the pressure calibrants: Ar, Ne, Au, or H_2O ice. Gray labels indicate peaks of the rhenium gasket. The stars in A are unresolved peaks that are possibly from FeOOH residual. Abbreviation: P, P-phase FeO_2Hx.

P phase from experiments were above that of FeO_2, but below the simulated curve for FeO_2H, consistent with the expected behavior of FeO_2Hx. The data scattering was an order of magnitude greater than the experimental uncertainty, clearly indicating the variable nonstoichiometry effect. Samples heated to higher temperature tend to have lower volumes, showing more hydrogen loss (Fig. 2, *Inset*).

To quantify the nonstoichiometry in FeO_2Hx, we first established the experimental equation of state (EOS) V_{e0i} of FeO_2 as a function of pressure for the baseline at ambient temperature as shown in Fig. 2. Although first-principles methods for studying transition metals suffer from strong correlation effects stemming from their *d* orbitals, which limits the accuracy in absolute values of volume and electronic structure (18, 19), the relative volume from the same simulation setup is reliable. Here we use the difference between the simulated FeO_2 and FeO_2H for the full range of *x* from 0 to 1. For an observed volume V_e, the amount of hydrogen *x* can thus be determined by the relation that combines theory and experiment,

$$x = \frac{V_e - V_{e0i}}{V_{s1i} - V_{s0i}}, \qquad [1]$$

where the subscripts *e*, *s*, 1*i*, and 0*i* denote the volume from experiment, from simulation, for $x = 1$ (FeO_2H), and for $x = 0$ (FeO_2), respectively, at the same pressure. In Fig. 2, the dashed curves are directly taken from the simulations, the dotted blue curve is the experimental EOS of FeO_2, and the dotted green curve represents $V_{e1i} = V_{e0i} + (V_{s1i} - V_{s0i})$. We observed increased dehydrogenation with increasing temperatures. For example, the composition at 87.5 GPa (quenched from 1,700 K, run no. 1603G266c) was $FeO_2H_{0.56}$. The same sample, by further heating to 2,150 K, caused the value of *x* to drop by 21% to $FeO_2H_{0.44}$ (run no. 1603G266d; Fig. 2, *Inset*). We also found that varying pressure alone did not change *x* to a significant degree. The final value of *x* resulted from a combination of temperature, heating time, and to a lesser degree, pressure. Throughout our experiments, we observed that *x* varies from 0.39 to 0.81 at different synthesis conditions (Table 1). The dehydrogenation of FeO_2H is thus described by the following chemical equation,

$$2FeO_2H = 2FeO_2Hx + (1-x)H_2,$$
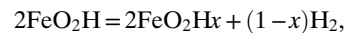
where *x* decreases (dehydrogenation) with temperature and time.

The volume variance was also investigated by the multigrain crystallography (MGC) method that had been adopted for high-pressure crystallographic studies (20, 21). This method is ideal for laser-heated samples that often result in multiple small single-crystal grains that then give spotty diffraction patterns. For a quenched sample at 110 GPa, we searched the ω range of −20° to +20° and at least 21 single crystals were identified by the MGC software (22). The statistics of all grains and crystallographic data for five selected grains are listed in Tables S1–S6. Those 21 grains stemmed from one set of multigrain data that covered only a volume of the synchrotron beam intersection area (beam size 0.8×2 μm²) times the depth along the beam direction (8–10 μm). The large 1.2% volume difference (equivalent to $x = 0.39 \sim 0.51$, Fig. 3) was more than an order of magnitude higher than refinement uncertainty. This result was reproduced by single-crystal data taken at other pressures. Because dehydrogenation requires diffusion of hydrogen from the center to the edge of the sample, such observation is readily interpreted by the diffusion gradient of *x* in FeO_2Hx at the time of synthesis. In the lower mantle conditions through geological time, it is reasonable to expect nearly complete dehydrogenation, i.e., $x \to 0$.

Table 1. Synthesis condition and results of FeO_2Hx

Run no.	Pressure, GPa	Temperature, K	Starting material	*a*, Å	*V*, Å³	*x*
1512G300	86.0	2,200	FeOOH in Ne	4.4152	21.517	0.59
1603G261	98.5	1,850	FeOOH in H_2O	4.3795	21.000	0.55
1603G270	109.0	2,250	$Fe_2O_3 + H_2O$	4.3383	20.413	0.43
1603G266a	72.0	2,300	$Fe_2O_3 + H_2O$	4.4424	21.918	0.54
1603G266b	78.5	2,300	$Fe_2O_3 + H_2O$	4.4238	21.643	0.53
1603G266c	89.0	1,700	$Fe_2O_3 + H_2O$	4.4025	21.332	0.56
1603G266d	87.5	2,150	$Fe_2O_3 + H_2O$	4.3877	21.118	0.44
1606G260	91.5	1,600	FeOOH in Ar	4.4330	21.779	0.81
1606GS02a	106.5	2,000	$Fe_2O_3 + H_2O$	4.3771	20.965	0.66
1606GS02b	133.5	2,000	$Fe_2O_3 + H_2O$	4.3276	20.262	0.69
1607G260	95.0	2,000	FeOOH in Ar	4.4178	21.556	0.76
1608GS02	119.0	2,500	FeOOH in Ne	4.3447	20.503	0.62

The formation of P phase was recognized in all experiments above 72 GPa. The table contains selected data in each run of synthesis after temperature quenching. Details of pressure calibration are in Table S7. The comprehensive data sheet is shown in Table S8.
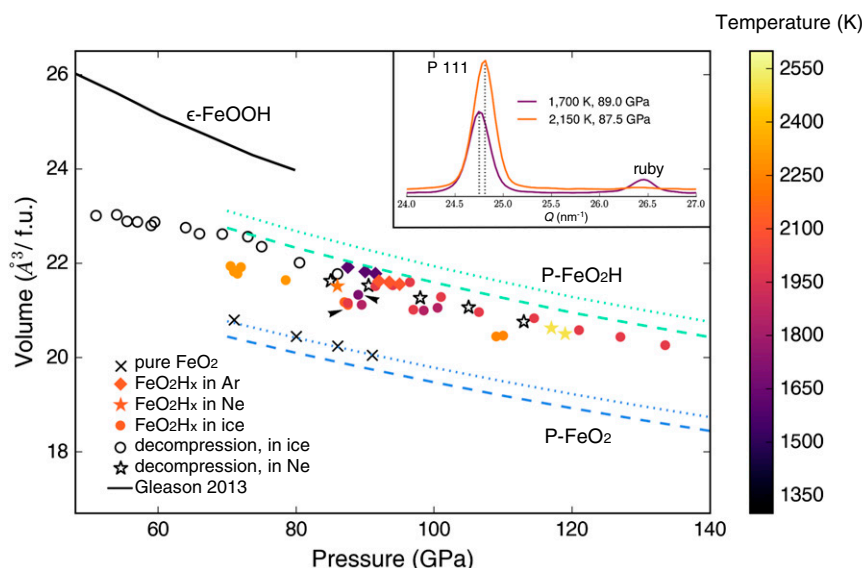
Hu et al.

Fig. 2. Volume vs. pressure for the P phase. Dashed lines are calculated from first-principles simulations. Blue dotted line is the experimental EOS of FeO_2. Green dotted line is the calibrated EOS V_{e1} from relative volume difference. Solid curve of ϵ-FeOOH is from ref. 14. The colors of the data points reflect the heating temperature, scaled into the color bar. All data points were collected after quenching. *Inset* shows the shift of P-phase 111 peak by raising the temperature from 1,700 K to 2,150 K, equivalent to a loss of 21% hydrogen. *Inset* data are indicated by black arrows in the main plot. Abbreviation: P, P phase. Q, momentum transfer.

Discussion

In the general concept of hydrogen circulating by hydration and dehydration, the hydrogen and water cycles are indistinguishable, and water does not affect the oxidation states. This concept may have to be revised by the observation of dehydrogenation of FeO_2H in this work, indicating the hydrogen cycle may couple to the redox reaction of the mantle.

Unlike the dehydration process that releases hydrogen as H_2O, hydrogen is reduced from dehydrogenation of FeO_2H and the FeO_2H is oxidized. In the FeO_2 peroxide (12), oxygen donates electrons to reduce both iron and hydrogen in this reaction, freeing hydrogen molecules and separating them from the cycling of water. In a general sense, when FeO_2H reaches below 1,800 km (75 GPa, 1,500 K in cold slab), the hydrogen and water cycles are separated through dehydrogenation. In conclusion, the dehydrogenation of FeO_2H represents an example that pressure can alter the hydration–dehydration cycle to become a redox reaction. The potential implications for this finding are that the effects of the hydrogen and water cycles must be considered separately under deep lower mantle conditions.

Materials and Methods

Preparation of Pure FeO_2. Pure FeO_2 was prepared from a starting assemblage of hematite and oxygen. Hematite powders were annealed at 1,000 °C for 24 h to eliminate any absorbed water. The dehydrated samples were placed on beveled diamond anvils of 150 µm in diameter to access near-megabar pressures. The sample chamber was a 50-µm-diameter hole drilled in a beryllium gasket supported by cubic-boron nitride padding. The DAC was placed in a sealed container immersed in liquid nitrogen. Oxygen gas was piped into the container and introduced into the sample chamber after it liquefied. Pyrite FeO_2 was synthesized by heating the sample at 75–91 GPa (1,700 ~ 2,000 K). The lattice parameter of pure FeO_2 is calibrated by indexing X-ray diffraction patterns collected at the synchrotron beam line of 16 insertion device B (ID-B), Advanced Photon Source (APS), Argonne National Laboratory (ANL). The results are consistent with our previous work (12).

Angular Dispersive X-Ray Diffraction Experiments. Angular dispersive X-ray diffraction experiments were performed at the 16-ID-B station of the High Pressure Collaborative Access Team (HPCAT) and the 13 bending magnet C (BM-C) station of the GeoSoilEnviroCARS (GSECARS), at the APS, ANL. Samples of hematite (annealed at 1,000 °C for 24 h) or goethite powders (no annealing) were precompressed to ~10 (thickness) × 30 (width) × 30 (length) µm³ before

loading into DAC. High pressure was achieved by using diamond anvils with 150-µm culet diameter (beveled from 300 µm) and the sample chamber was built in a drilled hole of 50–60 µm (diameter) in a rhenium gasket (23). For pressure medium of water, a droplet of deionized water was carefully injected into the chamber and immediately sealed. One or two pieces of ruby and a gold chip (when applicable) were placed around the sample to calibrate the pressure. At high pressure where ruby fluorescence becomes weak, pressure is calibrated by the EOS of Ne (24), Ar (25), Au (26), or ice (27). Details regarding the pressure calibration are listed in Table S7. The combined pressure uncertainty is ±2.0 GPa. The heating temperature was measured by fitting the black-body radiation curve on both sides of the sample. The laser spot is about 35 × 35 µm² at 2,600 K. Temperature gradients were still noticeable and we estimate up to 200 K uncertainty throughout our heating experiment (15).
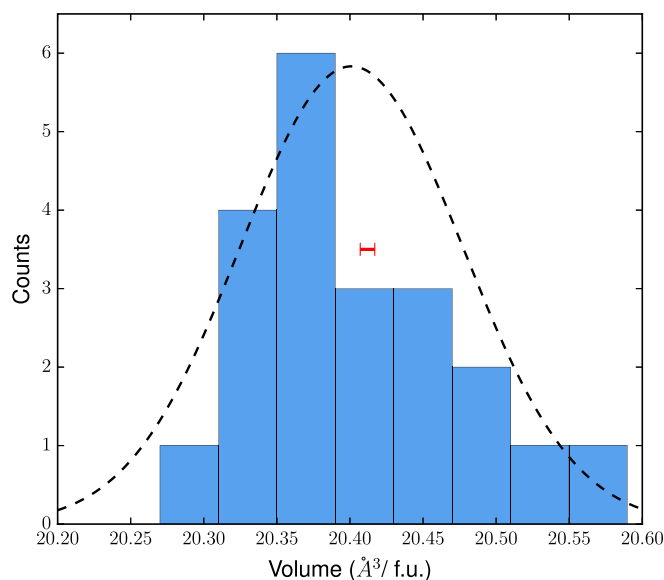

Fig. 3. Volume scattering in an FeO_2Hx multigrain sample at 110 GPa. The dashed line is the normal distribution of volume over all single-crystal grains, normalized by bin size and count number. The red bar indicates the volume 20.412(5) $Å^3$/formula unit (f.u.) solved from powder diffraction refinement.

First-Principles Simulations. EOS curves for FeO_2 and FeO_2H were calculated under the framework of density functional theory (DFT) implemented in the VASP code (28). To get rid of core charge overlap, we chose small-core pseudopotentials for O and H and standard potential for Fe within the Perdew, Burke, Ernzerhof (PBE) parameterization (29) of generalized gradient approximation (GGA) (30) for exchange correlation with a plane-wave basis set cutoff of 1,000 eV. The Brillouin zone was sampled by a uniform grid of $16 \times 16 \times 16$. To describe localized $3d$ electrons of Fe, DFT plus Hubbard part (U) (31) with a rotational invariant was used. In our previous theoretical study (32), we investigated an optimal value set of U (5 eV) (on-site Coulomb interaction) and J (0.8 eV) (Hund coupling constant) to properly describe the electronic structure of pyrite-type FeO_2 (32). The same parameters are used for FeO_2H and ε-FeOOH. Phonon dispersion of pyrite-FeOOH was calculated in a $2 \times 2 \times 2$ supercell, using the finite displacement method by Phonopy (33).

1. Jacobsen SD, van der Lee S (2006) *Earth's Deep Water Cycle* (Am Geophys Union, Washington, DC).
2. Williams Q, Hemley RJ (2001) Hydrogen in the deep earth. *Annu Rev Earth Planet Sci* 29:365–418.
3. Shieh SR, Duffy TS, Liu Z, Ohtani E (2009) High-pressure infrared spectroscopy of the dense hydrous magnesium silicates phase D and phase E. *Phys Earth Planet Inter* 175:106–114.
4. Suzuki A, Ohtani E, Kamada T (2000) A new hydrous phase δ-AlOOH synthesized at 21 GPa and 1000 °C. *Phys Chem Miner* 27(10):689–693.
5. Ohtani E, Litasov K, Suzuki A, Kondo T (2001) Stability field of new hydrous phase, δ-AlOOH, with implications for water transport into the deep mantle. *Geophys Res Lett* 28(20):3991–3993.
6. Nishi M, et al. (2014) Stability of hydrous silicate at high pressures and water transport to the deep lower mantle. *Nat Geosci* 7(3):224–227.
7. Tsuchiya J (2013) First principles prediction of a new high-pressure phase of dense hydrous magnesium silicates in the lower mantle. *Geophys Res Lett* 40(17):4570–4573.
8. Ohira I, et al. (2014) Stability of a hydrous δ-phase, AlOOH–MgSiO2(OH)2, and a mechanism for water transport into the base of lower mantle. *Earth Planet Sci Lett* 401:12–17.
9. Pamato MG, et al. (2015) Lower-mantle water reservoir implied by the extreme stability of a hydrous aluminosilicate. *Nat Geosci* 8(1):75–79.
10. Nishihara Y, Matsukage KN (2016) Iron-titanium oxyhydroxides as water carriers in the Earth's deep mantle. *Am Mineral* 101(4):919–927.
11. Yang X, Keppler H, Li Y (2016) Molecular hydrogen in mantle minerals. *Geochem Perspect Lett* 2:160–168.
12. Hu Q, et al. (2016) FeO2 and FeOOH under deep lower-mantle conditions and Earth's oxygen-hydrogen cycles. *Nature* 534(7606):241–244.
13. Gleason AE, Jeanloz R, Kunz M (2008) Pressure-temperature stability studies of FeOOH using X-ray diffraction. *Am Mineral* 93(11-12):1882–1885.
14. Gleason AE, Quiroga CE, Suzuki A, Pentcheva R, Mao WL (2013) Symmetrization driven spin transition in ε-FeOOH at high pressure. *Earth Planet Sci Lett* 379:49–55.
15. Meng Y, Hrubiak R, Rod E, Boehler R, Shen G (2015) New developments in laser-heated diamond anvil cell with in situ synchrotron x-ray diffraction at High Pressure Collaborative Access Team. *Rev Sci Instrum* 86(7):072201.
16. Tsuchiya J, Tsuchiya T (2011) First-principles prediction of a high-pressure hydrous phase of AlOOH. *Phys Rev B* 83(5):054115.
17. Speziale S, Jeanloz R, Milner A, Pasternak MP, Zaug JM (2005) Vibrational spectroscopy of Fe(OH)2 at high pressure: Behavior of the O-H bond. *Phys Rev B* 71(18):184106.
18. Kotliar G, et al. (2006) Electronic structure calculations with dynamical mean-field theory. *Rev Mod Phys* 78(3):865–951.
19. Eom T, Lim H-K, Goddard WA, Kim H (2015) First-principles study of iron oxide polytypes: Comparison of GGA+U and hybrid functional method. *J Phys Chem C* 119(1):556–562.
20. Zhang L, et al. (2016) *In-situ* crystal structure determination of seifertite SiO2 at 129 GPa: Studying a minor phase near Earth's core–mantle boundary. *Am Mineral* 101(1):231–234.
21. Zhang L, et al. (2014) Disproportionation of (Mg,Fe)SiO3 perovskite in Earth's deep lower mantle. *Science* 344(6186):877–882.
22. Sørensen HO, et al. (2012) Multigrain crystallography. *Z Kristallogr* 227:63–78.
23. Hrubiak R, Sinogeikin S, Rod E, Shen G (2015) The laser micro-machining system for diamond anvil cell experiments and general precision machining applications at the High Pressure Collaborative Access Team. *Rev Sci Instrum* 86(7):072202.
24. Fei Y, et al. (2007) Toward an internally consistent pressure scale. *Proc Natl Acad Sci USA* 104(22):9182–9186.
25. Ross M, Mao HK, Bell PM, Xu JA (1986) The equation of state of dense argon: A comparison of shock and static studies. *J Chem Phys* 85(2):1028–1033.
26. Anderson OL, Isaak DG, Yamamoto S (1989) Anharmonicity and the equation of state for gold. *J Appl Phys* 65(4):1534–1543.
27. Wolanin E, et al. (1997) Equation of state of ice VII up to 106 GPa. *Phys Rev B* 56(10):5781–5785.
28. Kresse G, Furthmüller J (1996) Efficient iterative schemes for ab initio total-energy calculations using a plane-wave basis set. *Phys Rev B Condens Matter* 54(16):11169–11186.
29. Perdew JP, Burke K, Ernzerhof M (1996) Generalized gradient approximation made simple. *Phys Rev Lett* 77(18):3865–3868.
30. Perdew JP, et al. (1992) Atoms, molecules, solids, and surfaces: Applications of the generalized gradient approximation for exchange and correlation. *Phys Rev B Condens Matter* 46(11):6671–6687.
31. Dudarev SL, Botton GA, Savrasov SY, Humphreys CJ, Sutton AP (1998) Electron-energy-loss spectra and the structural stability of nickel oxide: An LSDA+U study. *Phys Rev B* 57:1505.
32. Jang BG, Kim DY, Shim JH (2016) Metal-insulator transition and the role of electron correlation in FeO2. *arXiv*:1606.09582v2.
33. Togo A, Tanaka I (2015) First principle phonon calculations in materials science. *Scr Mater* 108:1–5.
34. Holland TJB, Redfern SAT (1997) UNITCELL: A nonlinear least-squares program for cell-parameter refinement and implementing regression and deletion diagnostics. *J Appl Cryst* 30(1):84.

EARTH, ATMOSPHERIC, AND PLANETARY SCIENCES